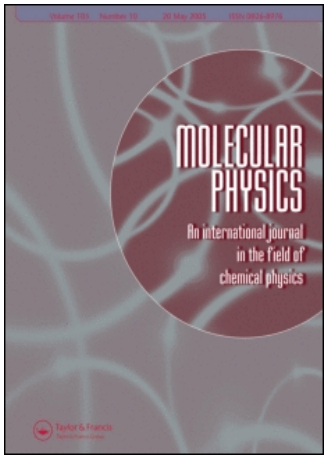

Molecular Physics
An International Journal in the Field of Chemical Physics
Publication details, including instructions for authors and subscription information:
http://www.informaworld.com/smpp/title~content=t713395160

High-resolution investigation of the excited electronic states of CaSH and SrSH by laser excitation spectroscopy - ARTICLE WITHDRAWN

Online Publication Date: 01 October 2006
To cite this Article: Sheridan, P. M., Dick, M. J., Wang, J. -G. and Bernath, P. F. (2006) 'High-resolution investigation of the excited electronic states of CaSH and SrSH by laser excitation spectroscopy - ARTICLE WITHDRAWN', Molecular Physics, 104:20, 3245 - 3259
To link to this article: DOI: 10.1080/00268970601075253
URL: http://dx.doi.org/10.1080/00268970601075253

Molecular Physics, Vol. 104, Nos. 20–21, 20 October–10 November 2006, 3245–3259

High-resolution investigation of the excited electronic states of CaSH and SrSH by laser excitation spectroscopy

P. M. SHERIDAN†, M. J. DICK, J.-G. WANG and P. F. BERNATH*‡
University of Waterloo, Ontario, Canada

(*Received 1 October 2006; in final form 13 October 2006*)

A laser ablation/pulsed molecular jet system has been used to record high-resolution laser excitation spectra of the $\tilde{C}^2A'$–$\tilde{X}^2A'$ transition of CaSH and the $\tilde{A}^2A'$–$\tilde{X}^2A'$, $\tilde{B}^2A''$–$\tilde{X}^2A'$, and $\tilde{C}^2A'$–$\tilde{X}^2A'$ transitions of SrSH. The rotationally-resolved data were analysed using an asymmetric top Hamiltonian (*A*-reduction) to determine rotational and fine structure parameters. A combined fit of all the newly measured and the previously recorded spectroscopic data for both CaSH and SrSH was performed. In the excited states observed in this study, both species were found to have a bent geometry. The spin-rotation parameters were analysed in terms of the pure precession and unique perturber approximations. In the excited electronic states of SrSH, the large spin-rotation interaction was found to cause perturbations between the $K_a = 0$ and 1 levels within each state. In the $\tilde{A}^2A'$ and $\tilde{B}^2A''$ states of both species, the metal-sulfur bond length was found to decrease relative to the ground state, which is consistent with previous observations of other calcium and strontium radicals.

1. Introduction

Among the small metal-containing molecules bonded to a single polyatomic ligand, the metal monohydroxides (MOH) have been the most investigated, both experimentally and theoretically [1, 2]. Extension of these studies to other polyatomic ligands, particularly those of lower symmetry, has been limited due to the complicated nature of their rotational energy level patterns and the difficulties associated with synthesizing them in sufficient quantities. One such species, the metal monohydrosulfides (MSH), is of interest because it is the sulfur analogue of the metal monohydroxides and therefore allows for comparison of the geometric and electronic properties between these two groups of molecules. For example, calcium, strontium, and barium monohydroxides have been found to possess linear geometries in their ground and low-lying electronic states [1]. This molecular structure has been attributed to the mostly ionic character of the metal–oxygen bond [3, 4]. In contrast, their hydrosulfide counterparts have not been found to share this characteristic. Limited spectroscopic data on the ground and low-lying excited electronic states of several of these species have shown that they are bent, with an M–S–H bond angle of ~90° [5]. This change in geometry is an indication of an increased covalent character in the metal–ligand bond [5]. Also, the reduced molecular symmetry of the metal hydrosulfides allows for additional interactions within and between their excited electronic states that are not possible for the metal hydroxides, making them of further interest [6].

The metal hydrosulfides were first observed in the gas phase by the Bernath group in their study of calcium and strontium monohydrosulfide and monothiolate derivatives [7]. Their low-resolution spectra suggested that CaSH and SrSH were non-linear in their four lowest energy electronic states. Subsequent high-resolution investigations of the $\tilde{A}^2A'$–$\tilde{X}^2A'$ [6] and $\tilde{B}^2A''$–$\tilde{X}^2A'$ [8] transitions of CaSH showed that this molecule was indeed bent in these states, in agreement with theoretical predictions [9, 10]. This work was followed by studies of the ground states of LiSH, NaSH, MgSH, CaSH, SrSH, BaSH, AlSH, and CuSH [5, 11–17] using pure rotational spectroscopic techniques. Again each of these molecules was found to possess a bent geometry in their ground state. Unfortunately, high-resolution studies of the

*Corresponding author. Email: pfb500@york.ac.uk
†Current Address: Department of Chemistry and Biochemistry, Canisius College, Buffalo, NY 14208, USA
‡Current Address: Department of Chemistry, University of York, Heslington, York, YO10 5DD, UK

Molecular Physics
ISSN 0026–8976 print/ISSN 1362–3028 online © 2006 Taylor & Francis
http://www.tandf.co.uk/journals
DOI: 10.1080/00268970601075253

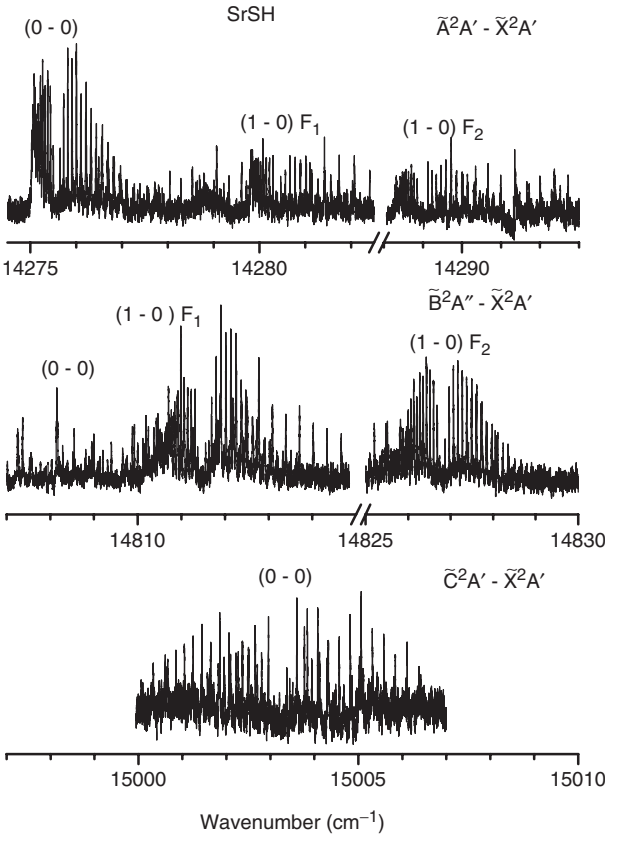

Figure 1. Overview of the spectra recorded for the $\tilde{A}^2A'$–$\tilde{X}^2A'$,$\tilde{B}^2A''$–$\tilde{X}^2A'$, and $\tilde{C}^2A'$–$\tilde{X}^2A'$ transitions of SrSH. Each subgroup of lines is labelled by the notation $(K'_a - K''_a)$. In the $\tilde{A}^2A'$–$\tilde{X}^2A'$ and $\tilde{B}^2A''$–$\tilde{X}^2A'$ transitions, multiple K_a subbands ((0–0) and (1–0)) were observed and each subband has the appearance of a perpendicular transition. In the $\tilde{C}^2A'$–$\tilde{X}^2A'$ transition only one subband (0–0) was observed, which has the structure of a parallel transition.

excited electronic states of the metal hydrosulfides have been limited to CaSH and to a recent report of the $\tilde{A}^2A''$–$\tilde{X}^2A'$ transition of CuSH [18].

In order to further examine the excited electronic states of the metal hydrosulfides, we have recorded high-resolution laser excitation spectra of the $\tilde{C}^2A'$–$\tilde{X}^2A'$ transition of CaSH along with the $\tilde{A}^2A'$–$\tilde{X}^2A'$, $\tilde{B}^2A''$–$\tilde{X}^2A'$, and $\tilde{C}^2A'$–$\tilde{X}^2A'$ transitions of SrSH. The rotationally-resolved spectra were analysed using an asymmetric top (*A*-reduction) Hamiltonian. Rotational and fine structure parameters were derived from a least-squares fit of the newly measured and the previously recorded spectroscopic data. CaSH and SrSH were both found to exhibit a bent geometry in each of the electronic states observed in this study. Evidence for electronic state mixing, an examination of the measured spin-rotation constants in terms of a pure precession model, and a comparison of excited state structural parameters for CaSH and SrSH will be presented.

2. Experimental

Laser excitation spectra of CaSH and SrSH were obtained using the laser ablation/pulsed molecular jet system of the Bernath group [19]. Ca and Sr vapour were produced by the ablation of a metal target rod (Ca or Sr) using the 3rd harmonic (355 nm) of a pulsed (10 Hz) Nd:YAG laser (10 mJ/pulse). The metal atoms reacted with a gas mixture of 7% H_2S in argon (100 psi backing pressure). The molecules then exited the pulsed nozzle assembly in a free jet expansion ($T_{rot} \sim 4$–6 K) and were interrogated ~15 cm downstream by a probe laser. A photomultiplier tube (PMT) was used to detect the laser-induced fluorescence and band pass filters (±20 nm) were employed to attenuate the plasma radiation. The output of the PMT was sent through a preamplifier (100× current) and then to a boxcar integrator for processing.

High-resolution laser excitation spectra of CaSH and SrSH were recorded using a Coherent ring dye (DCM laser dye) laser system. The band centres from previous low-resolution work [7] were used as the approximate starting positions for recording high-resolution spectra of each electronic transition. Rotationally resolved spectra were obtained in 5 cm^{-1} segments, at a data sampling interval of 10 MHz and scan speeds of 1–3 minutes per wavenumber, over the range of each transition. The slower scan speeds, and in some cases the averaging of several 5 cm^{-1} segments together, were necessary to increase the signal-to-noise ratio of the spectra. Line widths of approximately 350 MHz were observed and are the result of residual Doppler broadening in the molecular jet. The I_2 spectrum was recorded simultaneously by laser excitation spectroscopy with fluorescence detection and used to calibrate the spectra [20]. The estimated uncertainty of the spectral line positions is 0.003 cm^{-1}.

3. Results

The molecular geometry of CaSH and SrSH is bent. As a result these molecules can be classified as near prolate asymmetric tops belonging to the C_s point group. The electronic states of these species are ordered in energy as $\tilde{X}^2A'$, $\tilde{A}^2A'$, $\tilde{B}^2A''$, and $\tilde{C}^2A'$ [7, 10]. In the linear limit, the $\tilde{A}^2A'$ and $\tilde{B}^2A''$ terms correlate to a $^2\Pi$ state while the $\tilde{X}^2A'$ and $\tilde{C}^2A'$ terms correlate to $^2\Sigma^+$states [7]. Figure 1 shows an overview of the spectra recorded for the $\tilde{A}^2A'$–$\tilde{X}^2A'$, $\tilde{B}^2A''$–$\tilde{X}^2A'$, and $\tilde{C}^2A'$–$\tilde{X}^2A'$ transitions of SrSH. In the spectra of the $\tilde{A}^2A'$–$\tilde{X}^2A'$ and $\tilde{B}^2A''$–$\tilde{X}^2A'$ transitions, features arising from two $(K'_a - K''_a)$ subbands were observed. Both of these subbands, (0–0) and (1–0), have the appearance of perpendicular transitions.

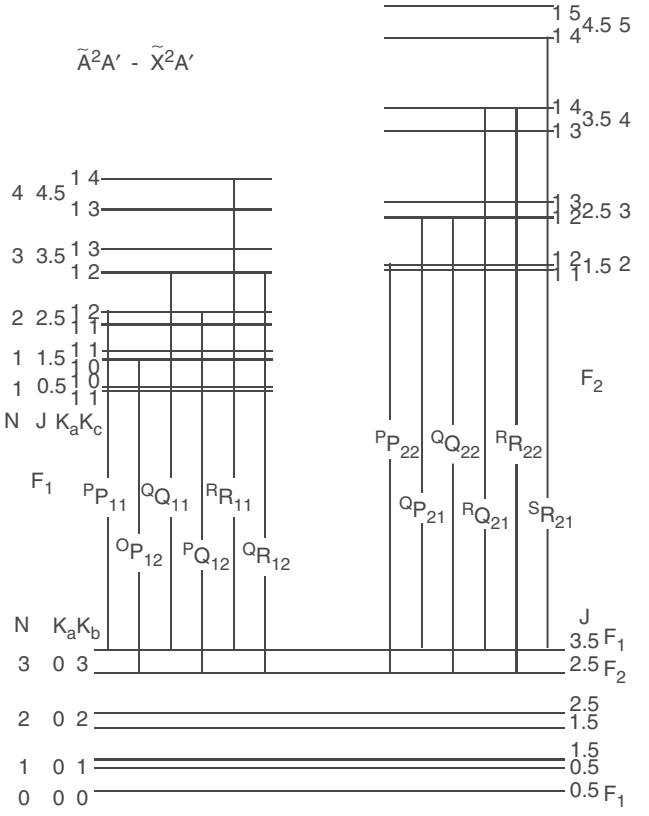

Figure 2. Energy level diagram of the $K'_a = 1 - K''_a = 0$ subband of the $\tilde{A}^2A'$–$\tilde{X}^2A'$ transition of CaSH and SrSH. Each rotational energy level is labelled by the quantities N, J, K_a, and K_c. The allowed transitions are determined by b-dipole type selections rules ($\Delta K_a = \pm 1$ and $\Delta K_c = \pm 1, \pm 3$) as well as $\Delta N = 0, \pm 1, \pm 2$ and $\Delta J = 0, \pm 1$. The rotational energy levels of the $\tilde{X}^2A'$ state have the appearance of a Hund's case (b) $^2\Sigma$ state and those of the $\tilde{A}^2A'$ state resemble a Hund's case (a) $^2\Pi$ (regular) state. A total of twelve branches are possible in this subband, labelled by the notation $^{\Delta N}\Delta J_{F'_iF''_j}(i = 1, 2; j = 1, 2)$.

For the $\tilde{C}^2A'$–$\tilde{X}^2A'$ transitions of CaSH and SrSH only the (0–0) subband was observed, which has the appearance of a parallel transition.

The rotational energy levels of CaSH and SrSH can be labelled using the asymmetric top molecule quantities K_a and K_c, which are the projections of the rotational angular momentum **N** onto the corresponding a and c inertial axes, respectively [21]. Because the metal hydrosulfides are near prolate asymmetric tops, their rotational energy levels can be grouped by the value of K_a. The rotational energy levels within each K_a group are split into two by asymmetry splitting and labelled by K_c, where $K_c = N - K_a$ or $N - K_a + 1$. In addition, CaSH and SrSH each possess an unpaired electron located primarily on the metal atom. Consequently, each asymmetry component of every rotational level is further split into two by the interaction of the unpaired electron spin (**S**) and the rotational angular momenta, and are labelled by **J**, where $\mathbf{J} = \mathbf{N} + \mathbf{S}$. Because CaSH and SrSH do not possess an axis of rotational symmetry and each has only a single hydrogen atom, proton nuclear spin statistics do not affect the K_a levels in these molecules [21]. Therefore, unlike in our previous study of $SrNH_2$ [22], only the rotational levels of the $K_a = 0$ component of the $\tilde{X}^2A'$ ground state are expected to be populated in our rotationally cold molecular jet.

An energy level diagram for the $K'_a = 1 - K''_a = 0$ subband of the $\tilde{A}^2A'$–$\tilde{X}^2A'$ transition of SrSH is shown in figure 2. Each energy level is identified by the quantum numbers N and J, as well as the asymmetric top labels K_a and K_c. The rotational energy levels of the $\tilde{X}^2A'$ ground state ($K_a = 0$) resemble a Hund's case (b) $^2\Sigma$ state. The spin-rotation parameters ε_{bb} and ε_{cc} (ε_{aa} is essentially zero) in this state are smaller than the rotational constants (B and C); therefore, the spin components (F_1 and F_2) can be grouped together by their value of N. For the $\tilde{A}^2A'$ state ($K_a = 1$) the rotational energy levels have the appearance of a Hund's case (a) $^2\Pi$ (regular) state. The splitting of the spin components in this state is much larger than in the ground state. In the $\tilde{A}^2\Pi$ state of the linear analogue SrOH, the F_1 and F_2 levels are separated by the spin-orbit coupling parameter A_{so} ($\sim 266\,cm^{-1}$) [23]. Because the $\tilde{A}^2A'$ state of SrSH is not orbitally-degenerate, the first-order contribution to this interaction is quenched. However, second-order spin-orbit coupling is possible. This effect can be significant and contributes to the ε_{aa} spin-rotation constant ($\sim 8.85\,cm^{-1}$), which is primarily responsible for the large splitting of the F_1 and F_2 components in the $\tilde{A}^2A'$ state. In this state, F_1 and F_2 designate the $\Sigma = -1/2$ and $+1/2$ spin components (Σ is the projection of **S** onto the symmetry axis in the linear limit), respectively. Because the inertial axis in SrSH is rotated by only 0.43° from the Sr–S bond, an approximate picture of the orbital character of the $\tilde{A}^2A'$ state can be extrapolated from species with higher molecular symmetry such as CaF and $CaNH_2$ [1]. The unpaired electron in the $\tilde{A}^2A'$ state resides in the in-plane component of a π orbital, which lies nearly along the molecular b-axis [6]. As a result, b-dipole type transitions ($\Delta K_a = \pm 1$ and $\Delta K_c = \pm 1, \pm 3$) are expected to be the most intense. The selection rules $\Delta N = 0, \pm 1, \pm 2$ and $\Delta J = 0, \pm 1$ give rise to twelve branches in the (1–0) subband, labelled by the notation $^{\Delta N}\Delta J_{F'_iF''_j}$ ($i = 1, 2$; $j = 1, 2$).

For the $\tilde{B}^2A''$–$\tilde{X}^2A'$ transition, an energy level diagram of the $K'_a = 1 - K''_a = 0$ subband is shown in figure 3. The ($K_a = 1$) rotational energy levels in the $\tilde{B}^2A''$ state have the appearance of a Hund's case (a) $^2\Pi$ (inverted) state due to the negative value of ε_{aa}. As a result, F_1 and F_2 now designate the $\Sigma = +1/2$ and $-1/2$ spin

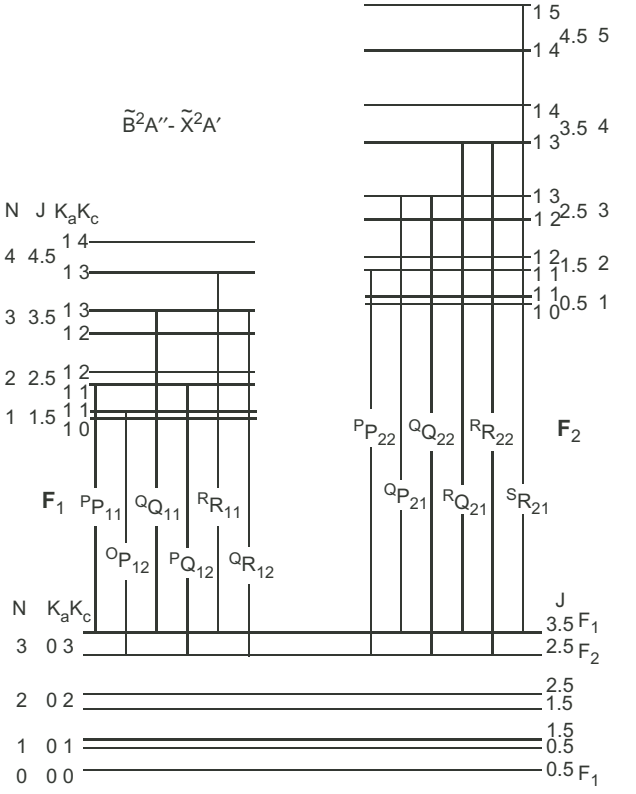

Figure 3. Energy level diagram of the $K'_a = 1 - K''_a = 0$ subband of the $\tilde{B}^2A''$–$\tilde{X}^2A'$ transition of CaSH and SrSH. The quantities N, J, K_a, and K_c are used to label each rotational energy level. The allowed transitions are determined by c-dipole type selections rules $\tilde{B}\Delta K_a = \pm 1$ and $\Delta K_c = 0, \pm 2$) as well as $\Delta N = 0$, ± 1, ± 2 and $\Delta J = 0$, ± 1. In the $\tilde{X}^2A'$ state, the rotational energy levels resemble a Hund's case (b) $^2\Sigma$ state while those of the $\tilde{B}^2A'$ state have the appearance of a Hund's case (a) $^2\Pi$ (inverted) state. In this subband a total of twelve branches are possible and are labeled by the notation $^{\Delta N}\Delta J_{F'_iF''_j}$ ($i = 1, 2$; $j = 1, 2$).

components, respectively. In the $\tilde{B}^2A''$ state, the unpaired electron (approximately) resides in a π orbital perpendicular to the plane of the molecule (molecular c-axis) [6]; therefore, c-dipole type transitions ($\Delta K_a = \pm 1$ and $\Delta K_c = 0$, ± 2) are expected to be the most intense. Twelve branches are possible in the (1–0) subband ($\Delta N = 0, \pm 1, \pm 2$ and $\Delta J = 0, \pm 1$) and are labelled by the notation $^{\Delta N}\Delta J_{F'_iF''_j}$ ($i = 1, 2$; $j = 1, 2$).

In the $\tilde{C}^2A'$ state, the unpaired electron resides in a σ-type molecular orbital. As a result, the most intense transitions expected between the $\tilde{C}^2A'$ and $\tilde{X}^2A'$ states of CaSH and SrSH are a-dipole type ($\Delta K_a = 0$; $\Delta K_c = \pm 1$, ± 3). Only transitions in the $K'_a = 0 - K''_a = 0$ subband, which has the appearance of a parallel type transition [22], are expected to be observed. Interestingly, features arising from the (0–0) subband were also observed in the $\tilde{A}^2A'$–$\tilde{X}^2A'$ and $\tilde{B}^2A''$–$\tilde{X}^2A'$ transitions of SrSH. This was surprising given the small degree of rotation of the inertial axes from the Sr–S bond. The presence of these subbands is due to the off-diagonal spin-rotation term in the Hamiltonian ($(\varepsilon_{ab} + \varepsilon_{ba})/2$), which can mix the rotational energy levels of the $K_a = 0$ and $K_a = 1$ levels [14, 16, 24]. In the $\tilde{A}^2A'$ and $\tilde{B}^2A''$ states of SrSH, this parameter is the same order of magnitude as the ε_{bb} and ε_{cc} spin-rotation constants; therefore, the $K_a = 0$ levels have sufficient $K_a = 1$ character to make the (0–0) subband observable. Because the ε_{bb} and ε_{cc} spin-rotation parameters are larger than the rotational constants in the $\tilde{A}^2A'$ and $\tilde{B}^2A''$ states of SrSH, the $K_a = 0$ rotational energy levels have the structure of a Hund's case (a) $^2\Pi$ state. As a result, the (0–0) subbands for the $\tilde{A}^2A'$–$\tilde{X}^2A'$ and $\tilde{B}^2A''$–$\tilde{X}^2A'$ transitions have the appearance of perpendicular transitions. Interestingly, we did not observe the (1–0) subbands in the $\tilde{C}^2A'$–$\tilde{X}^2A'$ transitions of CaSH and SrSH.

Quantum number assignments (J) for each transition of CaSH and SrSH were made using combination differences available from the ($K_a = 0$) ground state millimetre-wave data [14, 15]. Determination of the upper state K_a values for the $\tilde{A}^2A'$ and $\tilde{B}^2A''$ states was more complex, because, as mentioned previously, each group of lines has the appearance of a perpendicular transition. For the $\tilde{A}^2A'$–$\tilde{X}^2A'$ transition, the origin gap of the (1–0) F_2 subband is $\sim 4B$; therefore, the group of lines located at higher wavenumbers (see figure 1) was assigned to this subband. The remaining subbands ((1–0) F_1 and (0–0)) both have an origin gap of $\sim 2B$. However, the energy separation of the (0–0) band from the centre of the (1–0) F_1 and (1–0) F_2 spin components is given by the quantity $A'K'_a$. Using the value of the ground state A rotational constant as an estimate gives an energy separation of $\sim 10\,\mathrm{cm}^{-1}$. This condition is satisfied only if the group of lines on the lower wavenumber side of the spectrum is assigned as the (0–0) subband and those lines in the centre of the spectrum are assigned as the (1–0) F_1 subband. For the $\tilde{B}^2A''$–$\tilde{X}^2A'$ transition, the (1–0) F_1 subband has an origin gap of $\sim 4B$; therefore, the middle group of lines (see figure 1) could be assigned to this subband. Because the $K'_a = 0$ level lies lower in energy than the $K'_a = 1$ (F_2) level, the only plausible assignment for the weaker group of lines at lower wavenumbers is the (0–0) subband. The remaining stronger features at higher wavenumbers are the (1–0) F_2 subband. In addition, the similar intensity of the (1–0) F_1 and (1–0) F_2 spin-components in each electronic transition suggests that they share a common upper and lower K_a value.

In figure 4, a subsection of the $\tilde{A}^2A'$–$\tilde{X}^2A'$ spectrum of SrSH is presented with J assignments. In the top and bottom panels, the six branches observed for the (1–0) F_1 subband and the six branches of the (1–0) F_2 subband are shown, respectively. The overall appearance of the

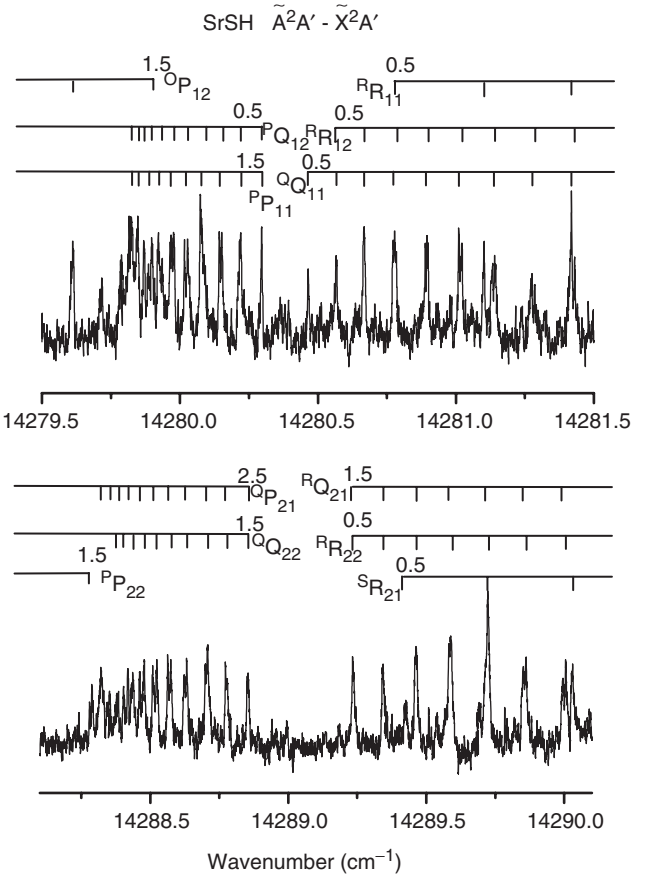

Figure 4. Expanded view of the (1–0) subbands of the $\tilde{A}^2A'$–$\tilde{X}^2A'$ transition of SrSH. Transitions involving the $K'_a = 1$, F_1 and F_2 spin components are shown in the top and bottom panels, respectively. In each spectrum, transitions arising from the six possible branches are presented and labelled by their J values. In the top panel the origin gap is $\sim 2B$, while in the bottom panel the origin gap is $\sim 4B$. Each spectrum has the appearance of a perpendicular transition with $\sim 1B$ and $\sim 3B$ spaced branches present.

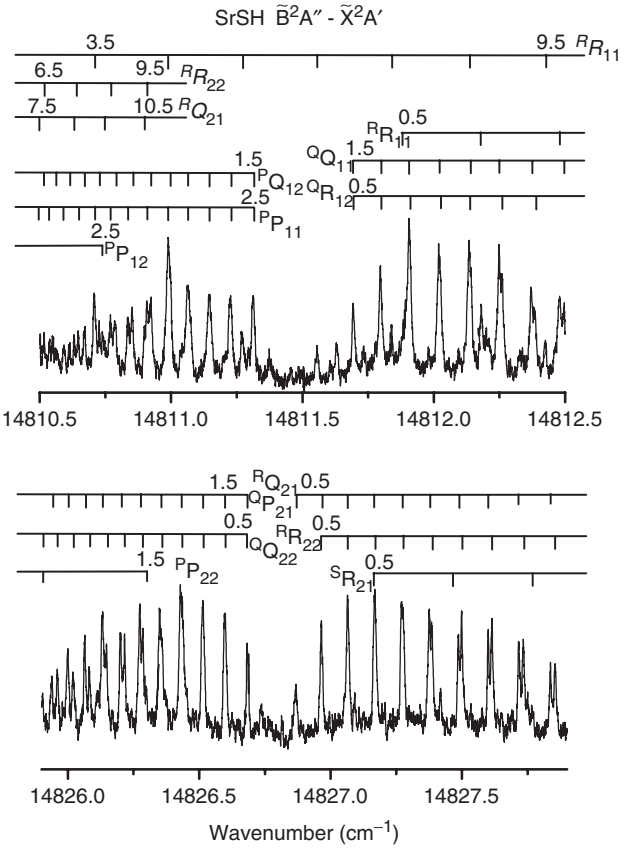

Figure 5. Expanded view of the $\tilde{B}^2A''$–$\tilde{X}^2A'$ transition of SrSH. In the top panel, the six branches of the (1–0) F_1 subband are shown along with three of the branches of the (0–0) subband (labelled in italics). In the bottom panel, the six branches observed for the (1–0) F_2 subband are shown. The origin gap of the (1–0) F_1 subband in the upper panel is $\sim 4B$, while in the lower panel the origin gap of the (1–0) F_2 subband is $\sim 2B$. The presence of $\sim 1B$ and $\sim 3B$ spaced branches in all three subbands gives each the appearance of a perpendicular transition.

spectra, with $\sim 1B$ and $\sim 3B$ spaced branches, is similar to a Hund's case (a) $^2\Pi$–Hund's case (b) $^2\Sigma$ transition. A portion of the $\tilde{B}^2A''$–$\tilde{X}^2A'$ spectrum of SrSH is displayed in figure 5, with quantum number assignments. In the top panel, transitions from three branches of the (0–0) subband (labelled in italics) are shown progressing through the six branches observed for the (1–0) F_1 subband. In the bottom panel, lines from the six branches of the (1–0) F_2 subband are presented. In each subband, a pattern of $\sim 1B$ and $\sim 3B$ spaced lines is present. Figure 6 shows a spectrum, with rotational assignments, of the (0–0) subband of the $\tilde{C}^2A'$–$\tilde{X}^2A'$ transition of SrSH. A total of six branches were observed in this subband, which exhibits the pattern of a Hund's case (b) $^2\Sigma$ – Hund's case (b) $^2\Sigma$ transition. The $\tilde{C}^2A'$–$\tilde{X}^2A'$ transition of CaSH, which is not shown, has a very similar appearance to that of SrSH.

4. Analysis

The rotational transitions recorded for the $\tilde{A}^2A'$–$\tilde{X}^2A'$, $\tilde{B}^2A''$–$\tilde{X}^2A'$, and $\tilde{C}^2A'$–$\tilde{X}^2A'$ transitions of SrSH and CaSH were fitted using a non-linear least-squares fitting program that contained the appropriate effective Hamiltonian in a Hund's case (b) basis. For the molecular rotation (A, B, and C) and its centrifugal distortion corrections (Δ_N, Δ_{NK}, higher order terms), matrix elements derived using Watson's asymmetric top Hamiltonian (A reduction) were used [25]. The spin-rotation interaction (A-reduction [26]) was modelled using the matrix elements given by Hirota [24]. For a molecule with C_s symmetry, there are four possible spin-rotation parameters: ε_{aa}, ε_{bb}, and ε_{cc} (diagonal) and the off-diagonal contribution $((\varepsilon_{ab} + \varepsilon_{ba})/2)$ [26].

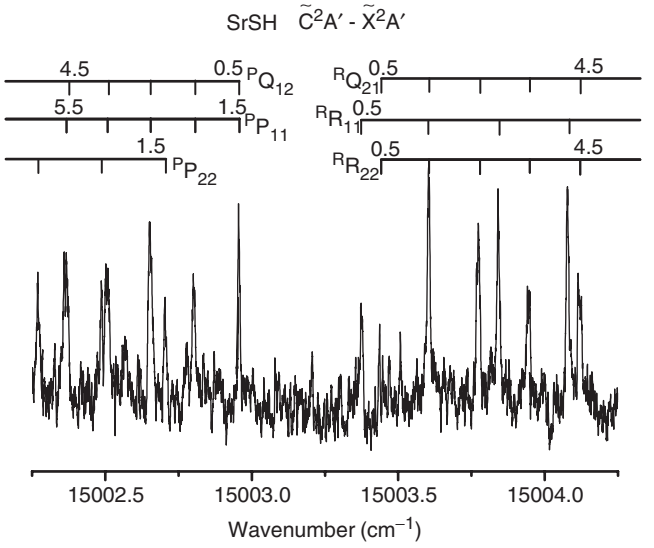

Figure 6. Expanded view of the $\tilde{C}^2A'$–$\tilde{X}^2A'$ transition of SrSH. The six branches of the (0–0) subband are shown with J values. This subband has the structure of a parallel type transition, with $\sim 2B$ spaced branches present. The $\tilde{C}^2A'$–$\tilde{X}^2A'$ transition of CaSH, which is not shown, has a similar appearance.

For CaSH 52 lines in the (0–0) subband of the $\tilde{C}^2A'$–$\tilde{X}^2A'$ transition were recorded. These data are available as supplemental material from the journal. A combined (weighted) fit of the $\tilde{C}^2A'$–$\tilde{X}^2A'$ data, in addition to the previous millimetre-wave data of the $\tilde{X}^2A'$ state ($0.0000015\,cm^{-1}$) [14] and $\tilde{A}^2A'$–$\tilde{X}^2A'$ ($0.005\,cm^{-1}$) [6] and $\tilde{B}^2A''$–$\tilde{X}^2A'$ ($0.004\,cm^{-1}$) [8] transitions was performed and the results are shown in table 1. The estimated errors for the lines used in the fits are given in parenthesis. Because of the limited data set for the $\tilde{C}^2A'$–$\tilde{X}^2A'$ transition, only the average values for the rotation ($(B+C)/2$) and spin-rotation ($(\varepsilon_{bb}+\varepsilon_{cc})/2$) parameters could be determined. In the $\tilde{C}^2A'$ state, the A rotational constant was fixed to the ground state value [14] and the ε_{aa} parameter was fixed to zero.

For SrSH, 195, 204, and 67 lines were measured for the $\tilde{A}^2A'$–$\tilde{X}^2A'$, $\tilde{B}^2A''$–$\tilde{X}^2A'$, and $\tilde{C}^2A'$–$\tilde{X}^2A'$ transitions, respectively. These data are available from the journal as supplemental material. A combined (weighted) fit of this data ($0.003\,cm^{-1}$) with the previously published millimetre wave data ($0.0000017\,cm^{-1}$) [15] was performed and the results are given in table 2. Because transitions involving both the (1–0) and (0–0) subbands were observed for the $\tilde{A}^2A'$–$\tilde{X}^2A'$ and $\tilde{B}^2A''$–$\tilde{X}^2A'$ transitions of SrSH, all three rotational constants along with the four spin-rotation parameters could be determined individually for the $\tilde{A}^2A'$ and $\tilde{B}^2A''$ states. Centrifugal distortion corrections to the rotational constants were not required for the $\tilde{A}^2A'$, $\tilde{B}^2A''$, and $\tilde{C}^2A'$ states due to the low J values observed in this work. For the $\tilde{B}^2A''$ state, however, the Δ^s_{KN} spin-rotation centrifugal distortion correction was found to improve the quality of the fit, suggesting a perturbation in the rotational energy levels of the $\tilde{B}^2A''$ state. For the $\tilde{C}^2A'$–$\tilde{X}^2A'$ transition of SrSH, again a limited data set was measured; therefore, only the average values of $((B+C)/2)$ and $((\varepsilon_{bb}+\varepsilon_{cc})/2)$ could be determined. Again, the A rotational parameter was fixed to the ground state value [15] and the ε_{aa} constant was fixed to zero.

5. Discussion

Calcium and strontium monohydrosulfide each possess an unpaired electron located on the metal atom. Because of the low molecular symmetry of these species, the resulting fine structure is modelled only as spin-rotation coupling. For heavy molecules, the first-order contribution to this interaction is generally negligible and second-order spin-orbit coupling effects tend to dominate [27]. The $\tilde{A}^2A'$,$\tilde{B}^2A''$, and $\tilde{C}^2A'$ states of calcium and strontium monohydrosulfide can be viewed, in the linear limit, as an interacting $p(\pi)/p(\sigma)$ complex. Therefore, using perturbation theory and the pure precession approximation, the second order contribution can be expressed as [28, 29]:

$$\varepsilon^{(2)}_{\alpha\alpha} = \sum_{n\neq 0} \frac{4B_\alpha \langle\psi_0|\hat{\ell}_\alpha|\psi_n\rangle\langle\psi_n|\zeta_{4p}\hat{\ell}_\alpha|\psi_0\rangle}{E^0_n - E^0_0} \qquad (1)$$

where α represents the principal axis system of the molecule ($B_a = A$, $B_b = B$, $B_c = C$), ζ_{4p} is the atomic spin-orbit constant for the $4p$ orbital of strontium ($3p$ in the case of calcium), and E_n and E_0 represent the energies ($v = 0$) of the interacting electronic states. Because the $\tilde{A}^2A'$, $\tilde{B}^2A''$, and $\tilde{C}^2A'$ states are sufficiently isolated from other interacting states, the unique perturber approximation can be utilized and the summation over n connecting states can be removed. Equation (1) can then be cyclically applied to obtain expressions for $\varepsilon^{(2)}_{\alpha\alpha}$ by considering which electronic states can interact as a result of a rotation of the molecule about the α axis. For $CaNH_2$, an asymmetric top molecule, expressions for each spin-rotation parameter in the three lowest-lying excited electronic states have been derived [29]. It is of interest to examine how well these equations apply to the excited states of the lower symmetry metal hydrosulfides.

The calculated second order spin-orbit contributions to the spin-rotation constants of CaSH and SrSH are presented in table 3. The measured values are also listed for comparison. In the $\tilde{A}^2A'$ state of CaSH, the

Table 1. Spectroscopic parameters (in cm^{-1}) for CaSH.[a]

Parameter[b]	$\tilde{X}^2A'$	$\tilde{A}^2A'$	$\tilde{B}^2A''$	$\tilde{C}^2A'$
T	0.0	15380.29079(23)	15859.46277(73)	16075.12884(65)
A	9.693540(45)	9.090954(77)	10.43552(78)	9.693540[c]
$(B+C)/2$	0.140741287(30)	0.14614820(33)	0.142292(13)	0.144783(15)
$(B-C)/2$	0.00116479(14)	0.0013285(10)	0.001151(75)	
Δ_K	$8.880(16)\times10^{-4}$	$4.630(36)\times10^{-4}$		
Δ_{NK}	$1.20491(84)\times10^{-5}$	$2.0039(21)\times10^{-5}$		
Δ_N	$1.00155(10)\times10^{-7}$	$1.2974(13)\times10^{-7}$		
δ_K	$9.216(55)\times10^{-6}$			
δ_N	$1.834(12)\times10^{-9}$			
Φ_{KN}	$4.77(11)\times10^{-9}$			
Φ_{NK}	$7.41(24)\times10^{-11}$			
ε_{aa}	−0.000583(99)	3.44584(26)	−5.77951(93)	0.0[d]
$(\varepsilon_{bb}+\varepsilon_{cc})/2$	0.00139806(49)	0.051688(16)	0.07010(23)	−0.05097(14)
$(\varepsilon_{bb}-\varepsilon_{cc})/2$	0.0001234(13)	−0.026603(29)	0.03751(36)	
$(\varepsilon_{ab}+\varepsilon_{ba})/2$	−0.00011281(53)	0.065929(46)		
Δ^s_{NK}		$3.48(58)\times10^{-5}$		
Δ^s_{KN}		$-4.93(76)\times10^{-4}$		
Δ^s_S		$-2.149(77)\times10^{-3}$		

[a]Combined fit includes previously recorded millimetre-wave [14], $\tilde{A}^2A'$–$\tilde{X}^2A'$ [6], and $\tilde{B}^2A''$–$\tilde{X}^2A'$ [8] transition data.
[b]Values in parenthesis are 1σ standard deviations, in units of the last significant digits.
[c]Fixed to the $\tilde{X}^2A'$ state value.
[d]Fixed to zero.

Table 2. Spectroscopic parameters (in cm^{-1}) for SrSH.[a]

Parameter[b]	$\tilde{X}^2A'$	$\tilde{A}^2A'$	$\tilde{B}^2A''$	$\tilde{C}^2A'$
T	0.0	14275.69327(64)	14809.61225(62)	15003.14682(60)
A	9.7179(19)	9.23006(79)	9.7334(30)	9.7179[c]
$(B+C)/2$	0.095448499(22)	0.0984682(40)	0.0969202(35)	0.0970991(87)
$(B-C)/2$	0.00054170(11)	0.00085(12)	0.00247(34)	
Δ_{NK}	$6.4809(16)\times10^{-6}$			
Δ_N	$4.62176(30)\times10^{-8}$			
δ_K	$5.157(37)\times10^{-6}$			
δ_N	$5.680(47)\times10^{-10}$			
Φ_{KN}	$4.306(84)\times10^{-9}$			
Φ_{NK}	$2.276(16)\times10^{-11}$			
L_K	$-2.276(14)\times10^{-11}$			
ε_{aa}	0.001740(82)	8.85191(58)	−15.1481(57)	0.0[d]
$(\varepsilon_{bb}+\varepsilon_{cc})/2$	0.0019214(38)	0.24009(10)	0.15852(15)	0.06983(11)
$(\varepsilon_{bb}-\varepsilon_{cc})/2$	−0.0000419(13)	−0.01632(31)	0.01144(74)	
$(\varepsilon_{ab}+\varepsilon_{ba})/2$	−0.000138(11)	0.1667(10)	0.1063(12)	
Δ^s_{KN}			$6.56(59)\times10^{-2}$	
Δ^s_N	$-1.14(32)\times10^{-9}$			

[a]Combined fit includes previously recorded millimetre-wave transition data [15].
[b]Values in parenthesis are 1σ standard deviations, in units of the last significant digits.
[c]Fixed to the $\tilde{X}^2A'$ state value.
[d]Fixed to zero.

measured value of ε_{aa} was found to be nearly $2\,cm^{-1}$ less than the calculated value. The discrepancy between the measured and calculated value of ε_{aa} in the $\tilde{A}^2A'$ state of CaSH was mainly attributed to 'orbital mixing' between the $\tilde{A}^2A'$ and $\tilde{C}^2A'$ states in the non-rotating molecule [6]. This interaction has the effect of lowering the effective orbital angular momentum of the unpaired electron in the $\tilde{A}^2A'$ state and increasing it in the $\tilde{C}^2A'$

Table 3. Calculated second-order contributions to the spin-rotation constants of CaSH and SrSH.

	CaSH			SrSH		
	$\tilde{A}^2A'$	$\tilde{B}^2A''$	$\tilde{C}^2A'$	$\tilde{A}^2A'$	$\tilde{B}^2A''$	$\tilde{C}^2A'$
$\varepsilon_{aa}^{(\mathrm{meas})}$	3.44584	−5.77951	0[a]	8.85191	−15.1481	0[a]
$\varepsilon_{aa}^{(2)}$	5.34	−5.34	0	19.4	−19.4	0
$\varepsilon_{bb}^{(\mathrm{meas})}$	0.025085	0.10761	−0.05097[b]	0.22377	0.16996	0.06983[b]
$\varepsilon_{bb}^{(2)}$	0	0.176	−0.176	0	0.528	−0.528
$\varepsilon_{cc}^{(\mathrm{meas})}$	0.078291	0.03259	−0.05097[b]	0.25641	0.14708	0.06983[b]
$\varepsilon_{cc}^{(2)}$	0.054	0	−0.054	0.139	0	−0.139

[a]Fixed to zero in the fit.
[b]$(\varepsilon_{bb}+\varepsilon_{cc})/2$.

state, which in turn affects the value of ε_{aa} in the same manner. This phenomenon also appears to be present in the $\tilde{A}^2A'$ state of SrSH, where the measured value of ε_{aa} is more than $10\,\mathrm{cm}^{-1}$ less than the calculated value. In contrast, for $CaNH_2$ and $SrNH_2$ the measured values of ε_{aa} in the $\tilde{A}^2B_2$ state were found to be in much better agreement with the calculated pure precession values, differing by only 0.043 and $0.018\,\mathrm{cm}^{-1}$, respectively [29, 30]. However, in $CaNH_2$ and $SrNH_2$ this orbital mixing interaction is not possible between the $\tilde{A}^2B_2$ and $\tilde{C}^2A_1$ states as they have different symmetries.

Table 3 also contains the calculated second order contributions to the ε_{bb} and ε_{cc} spin-rotation constants of CaSH and SrSH. For CaSH, the calculated values of these parameters in the $\tilde{A}^2A'$, $\tilde{B}^2A''$, and $\tilde{C}^2A'$ states are in relatively good agreement with the measured values. The slight differences most likely arise from the assumption of only p atomic orbital character being the dominant contribution to the molecular orbital of the unpaired electron in the excited electronic states. It is certainly possible that d atomic orbital character contributes to the make-up of these molecular orbitals [29].

For SrSH, however, the agreement between the calculated and measured ε_{bb} and ε_{cc} constants is not as good. Because of the large values of ε_{aa} in the $\tilde{A}^2A'$ and $\tilde{B}^2A''$ states of SrSH, the spin-components of the $K_a=0$ and 1 groups are close in energy in each state. In the $\tilde{A}^2A'$ state the $K_a=1$ (F_1 $\Sigma=-1/2$) level lies only $\sim 5\,\mathrm{cm}^{-1}$ higher in energy than the spin components of the $K_a=0$ level and in the $\tilde{B}^2A''$ state the separation of the $K_a=1$ (F_1 $\Sigma=+1/2$) level and the $K_a=0$ level is even smaller, $\sim 2\,\mathrm{cm}^{-1}$. The matrix elements for the $(\varepsilon_{ab}+\varepsilon_{ba})/2$ parameter mix the $K_a=0$ and 1 levels and the selection rule $\Delta\Sigma=0, \pm 1$ causes this interaction to be different for each of the spin components [24]. As a result, the energy positions of each of these spin components will be affected unequally, which in turn changes the measured value of the individual diagonal spin-rotation constants and is largely responsible for their deviation from the calculated values.

The large magnitude of the $(\varepsilon_{ab}+\varepsilon_{ba})/2$ constant in the $\tilde{A}^2A'$ and $\tilde{B}^2A''$ states can be interpreted in two different ways: either as a large rotation of the spin axes relative to the inertial axes or as a perturbation. In a molecule with C_s symmetry, the inertial a and b axes and the spin axes in the *a*-*b* plane can be rotated with respect to each other. In view of the similarity of the electronic structure of CaF and $CaNH_2$ with SrSH [1], a large rotation seems unrealistic. As a result, the interpretation of the large $(\varepsilon_{ab}+\varepsilon_{ba})/2$ parameter as a measure of an accidental internal perturbation between the $K_a=0$ and 1 levels in the $\tilde{A}^2A'$ and $\tilde{B}^2A''$ states of SrSH is more probable. In this case, the large off-diagonal spin-rotation parameter acts as an effective constant that accounts for this perturbation. In fact, the value of $(\varepsilon_{ab}+\varepsilon_{ba})/2$ in the $\tilde{A}^2A'$ and $\tilde{B}^2A''$ states is over 1000 times greater than in the ground state. In contrast, for CaSH where the value of ε_{aa} is smaller, the $K_a=0$ and 1 levels lie further apart in energy and the off-diagonal spin-rotation constant is an order of magnitude less in the $\tilde{A}^2A'$ state as compared to SrSH. In the $\tilde{B}^2A''$ state of CaSH a value for this parameter could not be determined from the data set observed in the molecular beam experiment [8].

In the $\tilde{C}^2A'$ state of SrSH, the ε_{bb} and ε_{cc} spin-rotation constants (the value of $(\varepsilon_{bb}+\varepsilon_{cc})/2$ is used for both ε_{bb} and ε_{cc}) differ in sign from the calculated value. As mentioned previously, the $\tilde{A}^2A'$ and $\tilde{C}^2A'$ states can now interact because they have the same symmetry. This interaction should increase the ε_{aa} constant in the $\tilde{C}^2A'$ state from the calculated value of zero to a positive value, shifting the $K_a=0$ and 1 levels closer together in energy. As was the case in the $\tilde{A}^2A'$ state, the close proximity in energy of the F_2 $K_a=1$ level to the $K_a=0$ levels allows them to perturb one another through the off-diagonal spin-rotation constant. In this case, the F_2 $K_a=0$ level is pushed lower in energy than the F_1 $K_a=0$ level, which results in a positive $(\varepsilon_{bb}+\varepsilon_{cc})/2$ parameter. As a result, a global fit of the rotational transitions of

Table 4. Second-order corrections to the rotational constants of CaSH and SrSH.

	CaSH			SrSH		
	$\tilde{A}^2A'$	$\tilde{B}^2A''$	$\tilde{C}^2A'$	$\tilde{A}^2A'$	$\tilde{B}^2A''$	$\tilde{C}^2A'$
$A^{(2)}$	0.7844	−0.7844	0	0.7075	−0.7075	0
A(meas)	9.090954	10.43552	9.693540[a]	9.23006	9.7334	9.7179[a]
$B^{(2)}$	0	+0.00037	−0.00037	0	+0.00019	−0.00019
B(meas)	0.1474767	0.143443	0.144783[b]	0.09932	0.09939	0.0970991[b]
$C^{(2)}$	0.00011	0	−0.00011	0.00005	0	−0.00005
C(meas)	0.1448197	0.141141	0.144783[b]	0.09762	0.09445	0.0970991[b]

the $K_a = 0$ and $K_a = 1$ levels would most likely not be possible for the $\tilde{C}^2A'$ state.

Another possible explanation for the positive value of $(\varepsilon_{bb} + \varepsilon_{cc})/2$ in the $\tilde{C}^2A'$ state of SrSH is an interaction between this state and one of the excited vibrational levels of the $\tilde{A}^2A'$ or $\tilde{B}^2A''$ states. A perturbation of this type was observed in the $K = 1$ levels of the $\tilde{B}^2A_1$ state of $CaCH_3$ [31]. Unfortunately, vibrational energy level information for the excited electronic states of SrSH is scarce. From the low-resolution investigation of SrSH, only a value for the Sr–S stretch (ν_3) of $\sim$270 cm^{-1} was determined for the $\tilde{X}^2A'$, $\tilde{A}^2A'$, and $\tilde{C}^2A'$ states [6]. Using this value, the $\nu_3 = 2$ and 3 vibrational levels in the $\tilde{A}^2A'$ state are calculated to lie approximately 100 cm^{-1} below and above the $\tilde{C}^2A'$ ($K_a = 0$) state. Assuming $\nu_3 = 270\,\text{cm}^{-1}$ for the $\tilde{B}^2A''$ state, $\nu_3 = 1$ lies $\sim$50 cm^{-1} higher in energy than the $\tilde{C}^2A'$ ($K_a = 0$) state. In addition, any quanta of the Sr–S stretch in the $\tilde{B}^2A''$ state would have the wrong symmetry to interact with the $\tilde{C}^2A'$ state. Theoretical calculations on the $\tilde{X}^2A'$ state of SrSH have given a value of $\sim$335 cm^{-1} for the bending mode (ν_2) [9]. Even assuming this value for the $\tilde{A}^2A'$ and $\tilde{B}^2A''$ states, no combination of ν_2 and ν_3 lies sufficiently close in energy to affect the $\tilde{C}^2A'$ ($K_a = 0$) state. As a result, this explanation is most likely not responsible for the change in sign of $(\varepsilon_{bb} + \varepsilon_{cc})/2$.

Second-order contributions to the rotational constants in the excited states of CaSH and SrSH are also possible [6, 29, 32]. These contributions have the general form [29]:

$$B^{(2)}_{\alpha\alpha} = \sum_{n \neq 0} \frac{4B^2_\alpha \left\langle \psi_0 | \hat{\ell}_\alpha | \psi_n \right\rangle^2}{E^0_0 - E^0_n} \qquad (2)$$

Using the unique perturber approximation, equation (2) can be simplified. Expressions for the second-order contributions to each of the rotational constants of the three low-lying excited electronic states of $CaNH_2$ have been derived [29]. As has been previously discussed for CaSH [6], a strong Coriolis interaction exists between the $\tilde{A}^2A'$ and $\tilde{B}^2A''$ states exists that significantly lowers and raises the A rotational constant in these states, respectively. Second-order contributions to the rotational constants must be taken into consideration in order to derive accurate structural parameters. The second-order contributions to the rotational constants in the $\tilde{A}^2A'$, $\tilde{B}^2A''$, and $\tilde{C}^2A'$ states of CaSH and SrSH are tabulated in table 4, along with the experimentally determined values for comparison. For CaSH and SrSH, the second-order corrections to the B and C rotational constants comprise less than 0.3% and 0.5% of the total measured value, respectively. For SrSH, similar to CaSH, large second-order contributions to the A rotational constant exist in the $\tilde{A}^2A'$ and $\tilde{B}^2A''$ states.

By removing the second order contributions to the rotational constants of the excited states of SrSH and CaSH, geometric parameters in these states can be calculated. The r_0 bond lengths (in Å) and bond angle (in degrees) for the $\tilde{A}^2A'$, $\tilde{B}^2A''$, and $\tilde{C}^2A'$ states of CaSH and SrSH, along with those of the $\tilde{X}^2A'$ state [11, 14], are tabulated in table 5. These parameters were calculated using the moment of inertia equations for a bent triatomic molecule [33]. Because only one isotopologue of CaSH and SrSH was studied in this work, the r_0 (S–H) bond length was held fixed to the ground state value in each excited state. Additionally for the $\tilde{C}^2A'$ states, the (M–S–H) bond angle was held fixed to the ground state value. As a result the calculated geometric parameters in each excited state are exact solutions to the moment of inertia equations. For both CaSH and SrSH, the r_0 (M–S) bond length is found to decrease in the $\tilde{A}^2A'$ and $\tilde{B}^2A''$ states as compared to the $\tilde{X}^2A'$ state value. A similar situation is found in the $\tilde{A}^2\Pi$ state of other linear calcium and strontium containing radicals [34]. This behaviour is thought to be due to the polarization of the unpaired electron away from the ligand, which in turn allows for an increase in the electrostatic interaction between the metal cation and anionic ligand. In the $\tilde{C}^2A'$ states, the r_0 (M–S) bond

Table 5. Structural parameters for CaSH and SrSH.

	CaSH				SrSH			
	$\tilde{X}^2A'$	$\tilde{A}^2A'$	$\tilde{B}^2A''$	$\tilde{C}^2A'$	$\tilde{X}^2A'$	$\tilde{A}^2A'$	$\tilde{B}^2A''$	$\tilde{C}^2A'$
r_0 (M–S) (Å)	2.564	2.517	2.550	2.562	2.706	2.665	2.686	2.720
r_0 (S–H) (Å)	1.357	1.357[a]	1.357[a]	1.357[a]	1.359	1.359[a]	1.359[a]	1.359[a]
θ (M–S–H) (°)	91.0	89.1	89.1	91.0[a]	91.0	89.1	89.1	91.0[a]

[a]Fixed to the $\tilde{X}^2A'$ state value.

lengths remain essentially unchanged from the ground state value. Caution of course must be used in interpreting these structural parameters considering the assumptions involved in their derivation. High-resolution spectra of isotopologues of these species would be useful in determining these structural parameters more precisely.

Acknowledgements

Financial support for this work was provided by the Natural Sciences and Engineering Research Council (NSERC) of Canada. The authors would like to thank Dr K. A. Walker for the loan of her Nd:YAG laser while ours was being repaired.

References

[1] P. F. Bernath, *Advances in Photochemistry* (Wiley, New York, 1997), Vol. 23, p. 1.
[2] A. M. Ellis, Int. Rev. Phys. Chem. **20,** 551 (2001).
[3] C. W. Bauschlicher Jr and H. Partridge, Chem. Phys. Lett. **106,** 65 (1984).
[4] C. W. Bauschlicher Jr, S. R. Langhoff, and H. Partridge, J. Chem. Phys. **84,** 901 (1986).
[5] A. Janczyk, S. K. Walter, and L. M. Ziurys, Chem. Phys. Lett. **401,** 211 (2005).
[6] C. N. Jarman and P. F. Bernath, J. Chem. Phys. **98,** 6697 (1993).
[7] W. T. M. L. Fernando, R. S. Ram, L. C. O'Brien, and P. F. Bernath, J. Phys. Chem. **95,** 2665 (1991).
[8] C. T. Scurlock, T. Henderson, S. Bosely, K. Y. Jung, and T. C. Steimle, J. Chem. Phys. **100,** 5481 (1994).
[9] W. T. Chan and I. P. Hamilton, Chem. Phys. Lett. **297,** 217 (1998).
[10] J. V. Ortiz, Chem. Phys. Lett. **169,** 116 (1990).
[11] A. Janczyk and L. M. Ziurys, Chem. Phys. Lett. **365,** 514 (2002).
[12] E. Kagi and K. Kawaguchi, Astrophys. J. **491,** L129 (1997).
[13] A. Taleb-Bendiab and D. Chomiak, Chem. Phys. Lett. **334,** 195 (2001).
[14] A. Taleb-Bendiab, F. Scappini, T. Amano, and J. K. G. Watson, J. Chem. Phys. **104,** 7431 (1996).
[15] D. T. Halfen, A. J. Apponi, J. M. Thompsen, and L. M. Ziurys, J. Chem. Phys. **115,** 11131 (2001).
[16] A. Janczyk and L. M. Ziurys, J. Chem. Phys. **119,** 10702 (2003).
[17] A. Janczyk and L. M. Ziurys, Astrophys. J. **639,** L107 (2006).
[18] F. Sunahori, X. P. Zhang, and D. Clouthier, J. Chem. Phys. **125,** 084310-1 (2006).
[19] C. Zhao, P. G. Hajigeorgiou, P. F. Bernath, and J. W. Hepburn, J. Mol. Spectrosc. **176,** 268 (1996).
[20] S. Gerstenkorn and P. Luc, *Atlas du Spectre d'Absorption de la Molécule d' Iode* (Laboratoire Aimé – Cotton, CNRS 91405, Orsay, France, 1978).
[21] C. H. Townes and A. L. Schawlow, *Microwave Spectroscopy* (Dover, New York, 1975).
[22] P. M. Sheridan, M. J. Dick, J.-G. Wang, and P. F. Bernath, J. Mol. Spectrosc. **233,** 269 (2005).
[23] J.-G. Wang, P. M. Sheridan, M. J. Dick, and P. F. Bernath, J. Mol. Spectrosc. **236,** 21 (2006).
[24] E. Hirota, *High-resolution Spectroscopy of Transient Molecules* (Springer-Verlag Series in Chemical Physics, Berlin, 1985).
[25] J. K. G. Watson, in *Vibrational Spectra and Structure*, edited by J. R. Durig (Elsevier, Amsterdam, 1977), p. 1.
[26] J. M. Brown and T. J. Sears, J. Mol. Spectrosc. **75,** 111 (1979).
[27] H. Lefebvre-Brion and R. W. Field, *The Spectra and Dynamics of Diatomic Molecules* (Elsevier, Amsterdam, 2004).
[28] R. N. Dixon, Mol. Phys. **10,** 1 (1965).
[29] Z. Morbi, C. Zhao, and P. F. Bernath, J. Chem. Phys. **106,** 4860 (1997).
[30] C. R. Brazier and P. F. Bernath, J. Mol. Spectrosc. **201,** 116 (2000).
[31] P. M. Sheridan, M. J. Dick, J.-G. Wang, and P. F. Bernath, J. Phys. Chem. A **109,** 10547 (2005).
[32] C. J. Whitham and Ch. Jungen, J. Chem. Phys. **93,** 1001 (1990).
[33] W. Gordy and R. L. Cook, *Microwave Molecular Spectra* (Wiley, New York, 1970).
[34] M. J. Dick, P. M. Sheridan, J.-G. Wang, and P. F. Bernath, J. Mol. Spectrosc. **233,** 197 (2005).

Supplementary Material

Table S1. Measured Data for the $A2A' - X2A'$, $B2A''$–$X2A'$, and $C2A'$–$X2A'$ transitions of SrSH and the $C2A'$–$X2A'$ transition of CaSH.

$J = J$
GAM = $N - Ka + Kc$
F = spin component 1 = F1 or 2 = F2
$Ka = Ka$
OBS = observed transition frequency in wavenumbers
OMC = observed transition frequency minus calculated transition frequency in wavenumbers

SrSH				$A2A'$–$X2A'$					
J	GAM	F	Ka	J	GAM	F	Ka	OBS	OMC
0.5	0	1	1	0.5	0	2	0	14280.2969	0.0011
1.5	1	1	1	1.5	0	2	0	14280.2231	0.0037
2.5	1	1	1	2.5	0	2	0	14280.1543	0.0048
3.5	1	1	1	3.5	0	2	0	14280.0896	0.0034
4.5	1	1	1	4.5	0	2	0	14280.0293	−0.0003
5.5	1	1	1	5.5	0	2	0	14279.9844	0.0049
6.5	1	1	1	6.5	0	2	0	14279.9371	0.0010
7.5	1	1	1	7.5	0	2	0	14279.8983	−0.0012
8.5	1	1	1	8.5	0	2	0	14279.8712	0.0017
9.5	1	1	1	9.5	0	2	0	14279.8468	0.0005
10.5	1	1	1	10.5	0	2	0	14279.8261	−0.0037
11.5	1	1	1	11.5	0	2	0	14279.8163	−0.0038
12.5	1	1	1	12.5	0	2	0	14279.8163	−0.0008
1.5	1	1	1	0.5	0	1	0	14280.7843	−0.0049
2.5	1	1	1	1.5	0	1	0	14281.1014	0.0022
3.5	1	1	1	2.5	0	1	0	14281.4187	0.0029
4.5	1	1	1	3.5	0	1	0	14281.7443	0.0054
5.5	1	1	1	4.5	0	1	0	14282.0732	0.0045
6.5	1	1	1	5.5	0	1	0	14282.4028	−0.0024
7.5	1	1	1	6.5	0	1	0	14282.7495	0.0012
8.5	1	1	1	7.5	0	1	0	14283.0988	0.0006
9.5	1	1	1	8.5	0	1	0	14283.4531	−0.0016
10.5	1	1	1	9.5	0	1	0	14283.8171	−0.0009
0.5	0	1	1	1.5	0	1	0	14280.2969	0.0040
1.5	1	1	1	2.5	0	1	0	14280.2231	0.0085
2.5	1	1	1	3.5	0	1	0	14280.1444	0.0016
3.5	1	1	1	4.5	0	1	0	14280.0781	0.0005
4.5	1	1	1	5.5	0	1	0	14280.0164	−0.0026
5.5	1	1	1	6.5	0	1	0	14279.9673	0.0003
6.5	1	1	1	7.5	0	1	0	14279.9206	−0.0011
7.5	1	1	1	8.5	0	1	0	14279.8859	0.0028
8.5	1	1	1	9.5	0	1	0	14279.8468	−0.0045
9.5	1	1	1	10.5	0	1	0	14279.8261	0.0000
10.5	1	1	1	11.5	0	1	0	14279.8133	0.0056
11.5	1	1	1	12.5	0	1	0	14279.7873	−0.0087
0.5	1	1	1	0.5	0	1	0	14280.4642	−0.0040
1.5	0	1	1	1.5	0	1	0	14280.5651	0.0010
2.5	0	1	1	2.5	0	1	0	14280.6659	−0.0006
3.5	0	1	1	3.5	0	1	0	14280.7726	−0.0026
4.5	0	1	1	4.5	0	1	0	14280.8894	−0.0009
5.5	0	1	1	5.5	0	1	0	14281.0103	−0.0014
6.5	0	1	1	6.5	0	1	0	14281.1334	−0.0060
7.5	0	1	1	7.5	0	1	0	14281.2735	0.0002
8.5	0	1	1	8.5	0	1	0	14281.4187	0.0052
9.5	0	1	1	9.5	0	1	0	14281.5613	0.0014
10.5	0	1	1	10.5	0	1	0	14281.7113	−0.0011
12.5	0	1	1	12.5	0	1	0	14282.0332	−0.0025
1.5	0	1	1	0.5	0	2	0	14280.5651	−0.0019
2.5	0	1	1	1.5	0	2	0	14280.6659	−0.0054
3.5	0	1	1	2.5	0	2	0	14280.7843	0.0024
4.5	0	1	1	3.5	0	2	0	14280.8947	−0.0042
5.5	0	1	1	4.5	0	2	0	14281.0226	0.0003
6.5	0	1	1	5.5	0	2	0	14281.1481	−0.0038
7.5	0	1	1	6.5	0	2	0	14281.2853	−0.0025
8.5	0	1	1	7.5	0	2	0	14281.4328	0.0030
9.5	0	1	1	8.5	0	2	0	14281.5800	0.0019
10.5	0	1	1	9.5	0	2	0	14281.7336	0.0011
12.5	0	1	1	11.5	0	2	0	14282.0616	0.0019
0.5	1	1	1	1.5	0	2	0	14279.8983	−0.0001
1.5	0	1	1	2.5	0	2	0	14279.6104	−0.0041
2.5	0	1	1	3.5	0	2	0	14279.3375	0.0006
3.5	0	1	1	4.5	0	2	0	14279.0670	0.0012
4.5	0	1	1	5.5	0	2	0	14278.7980	−0.0031
5.5	0	1	1	6.5	0	2	0	14278.5380	−0.0046
6.5	0	1	1	7.5	0	2	0	14278.2872	−0.0033
7.5	0	1	1	8.5	0	2	0	14278.0435	−0.0012
8.5	0	1	1	9.5	0	2	0	14277.8121	0.0070
9.5	0	1	1	10.5	0	2	0	14277.5786	0.0069
10.5	0	1	1	11.5	0	2	0	14277.3399	−0.0045
1.5	0	2	1	2.5	0	1	0	14288.8545	0.0035
2.5	0	2	1	3.5	0	1	0	14288.7721	0.0018
3.5	0	2	1	4.5	0	1	0	14288.7007	0.0048
4.5	0	2	1	5.5	0	1	0	14288.6220	−0.0057
5.5	0	2	1	6.5	0	1	0	14288.5624	−0.0034
6.5	0	2	1	7.5	0	1	0	14288.5088	−0.0013
7.5	0	2	1	8.5	0	1	0	14288.4621	0.0015
8.5	0	2	1	9.5	0	1	0	14288.4191	0.0017
9.5	0	2	1	10.5	0	1	0	14288.3846	0.0042
10.5	0	2	1	11.5	0	1	0	14288.3527	0.0030
11.5	0	2	1	12.5	0	1	0	14288.3206	−0.0046
12.5	0	2	1	13.5	0	1	0	14288.3134	0.0064
13.5	0	2	1	14.5	0	1	0	14288.2887	−0.0063
14.5	0	2	1	15.5	0	1	0	14288.2887	−0.0006
15.5	0	2	1	16.5	0	1	0	14288.2887	−0.0012
1.5	0	2	1	1.5	0	2	0	14288.8545	−0.0013
2.5	0	2	1	2.5	0	2	0	14288.7792	0.0022
3.5	0	2	1	3.5	0	2	0	14288.7093	0.0048
4.5	0	2	1	4.5	0	2	0	14288.6319	−0.0064
5.5	0	2	1	5.5	0	2	0	14288.5753	−0.0030
6.5	0	2	1	6.5	0	2	0	14288.5223	−0.0022
7.5	0	2	1	7.5	0	2	0	14288.4794	0.0024
8.5	0	2	1	8.5	0	2	0	14288.4375	0.0018
9.5	0	2	1	9.5	0	2	0	14288.4031	0.0025
10.5	0	2	1	10.5	0	2	0	14288.3772	0.0054
11.5	0	2	1	11.5	0	2	0	14288.3527	0.0035
12.5	0	2	1	12.5	0	2	0	14288.3305	−0.0024
13.5	0	2	1	13.5	0	2	0	14288.3206	−0.0023

(*continued*)

Table S1. Continued.

J	GAM	F	*Ka*	*J*	GAM	F	*Ka*	OBS	OMC
14.5	0	2	1	14.5	0	2	0	14288.3206	0.0015
15.5	0	2	1	15.5	0	2	0	14288.3206	−0.0010
1.5	0	2	1	0.5	0	1	0	14289.4265	0.0009
2.5	0	2	1	1.5	0	1	0	14289.7241	−0.0026
3.5	0	2	1	2.5	0	1	0	14290.0292	−0.0049
4.5	0	2	1	3.5	0	1	0	14290.3496	0.0019
5.5	0	2	1	4.5	0	1	0	14290.6651	−0.0024
6.5	0	2	1	5.5	0	1	0	14290.9922	−0.0014
7.5	0	2	1	6.5	0	1	0	14291.3231	−0.0027
8.5	0	2	1	7.5	0	1	0	14291.6577	−0.0066
9.5	0	2	1	8.5	0	1	0	14292.0070	−0.0021
10.5	0	2	1	9.5	0	1	0	14292.3650	0.0050
11.5	0	2	1	10.5	0	1	0	14292.7217	0.0045
1.5	1	2	1	1.5	0	1	0	14289.2358	0.0020
2.5	1	2	1	2.5	0	1	0	14289.3416	−0.0025
3.5	1	2	1	3.5	0	1	0	14289.4634	0.0027
4.5	1	2	1	4.5	0	1	0	14289.5824	−0.0013
5.5	1	2	1	5.5	0	1	0	14289.7151	0.0020
6.5	1	2	1	6.5	0	1	0	14289.8508	0.0018
7.5	1	2	1	7.5	0	1	0	14289.9959	0.0047
8.5	1	2	1	8.5	0	1	0	14290.1388	−0.0012
9.5	1	2	1	9.5	0	1	0	14290.2961	0.0009
10.5	1	2	1	10.5	0	1	0	14290.4572	0.0002
11.5	1	2	1	11.5	0	1	0	14290.6269	0.0016
12.5	1	2	1	12.5	0	1	0	14290.8052	0.0049
13.5	1	2	1	13.5	0	1	0	14290.9824	0.0006
1.5	1	2	1	0.5	0	2	0	14289.2358	−0.0009
2.5	1	2	1	1.5	0	2	0	14289.3416	−0.0073
3.5	1	2	1	2.5	0	2	0	14289.4634	−0.0041
4.5	1	2	1	3.5	0	2	0	14289.5900	−0.0024
5.5	1	2	1	4.5	0	2	0	14289.7241	0.0004
6.5	1	2	1	5.5	0	2	0	14289.8631	0.0016
7.5	1	2	1	6.5	0	2	0	14290.0058	0.0001
8.5	1	2	1	7.5	0	2	0	14290.1571	0.0008
9.5	1	2	1	8.5	0	2	0	14290.3159	0.0024
10.5	1	2	1	9.5	0	2	0	14290.4781	0.0009
11.5	1	2	1	10.5	0	2	0	14290.6479	0.0005
12.5	1	2	1	11.5	0	2	0	14290.8254	0.0011
13.5	1	2	1	12.5	0	2	0	14291.0039	−0.0039
1.5	1	2	1	2.5	0	2	0	14288.2801	−0.0040
0.5	0	1	0	1.5	0	1	0	14275.5022	0.0008
1.5	0	1	0	2.5	0	1	0	14275.4360	0.0011
2.5	0	1	0	3.5	0	1	0	14275.3759	0.0025
3.5	0	1	0	4.5	0	1	0	14275.3202	0.0033
4.5	0	1	0	5.5	0	1	0	14275.2661	0.0006
5.5	0	1	0	6.5	0	1	0	14275.2193	0.0003
6.5	0	1	0	7.5	0	1	0	14275.1752	−0.0025
7.5	0	1	0	8.5	0	1	0	14275.1392	−0.0021
8.5	0	1	0	9.5	0	1	0	14275.1064	−0.0035
9.5	0	1	0	10.5	0	1	0	14275.0841	0.0005
10.5	0	1	0	11.5	0	1	0	14275.0596	−0.0028
11.5	0	1	0	12.5	0	1	0	14275.0473	0.0011
12.5	0	1	0	13.5	0	1	0	14275.0350	−0.0001
0.5	0	1	0	0.5	0	2	0	14275.5022	−0.0021
1.5	0	1	0	1.5	0	2	0	14275.4360	−0.0037

Table S1. Continued.

J	GAM	F	*Ka*	*J*	GAM	F	*Ka*	OBS	OMC
2.5	0	1	0	2.5	0	2	0	14275.3821	0.0020
3.5	0	1	0	3.5	0	2	0	14275.3273	0.0017
4.5	0	1	0	4.5	0	2	0	14275.2784	0.0024
5.5	0	1	0	5.5	0	2	0	14275.2317	0.0002
6.5	0	1	0	6.5	0	2	0	14275.1923	0.0002
7.5	0	1	0	7.5	0	2	0	14275.1555	−0.0021
8.5	0	1	0	8.5	0	2	0	14275.1259	−0.0023
9.5	0	1	0	9.5	0	2	0	14275.1064	0.0026
10.5	0	1	0	10.5	0	2	0	14275.0841	−0.0004
11.5	0	1	0	11.5	0	2	0	14275.0711	0.0009
12.5	0	1	0	12.5	0	2	0	14275.0596	−0.0014
13.5	0	1	0	13.5	0	2	0	14275.0596	0.0027
1.5	0	2	0	0.5	0	2	0	14275.7262	−0.0051
2.5	0	2	0	1.5	0	2	0	14275.8171	−0.0011
3.5	0	2	0	2.5	0	2	0	14275.9082	−0.0019
4.5	0	2	0	3.5	0	2	0	14276.0091	0.0020
5.5	0	2	0	4.5	0	2	0	14276.1052	−0.0041
6.5	0	2	0	5.5	0	2	0	14276.2206	0.0039
7.5	0	2	0	6.5	0	2	0	14276.3290	−0.0003
8.5	0	2	0	7.5	0	2	0	14276.4422	−0.0049
9.5	0	2	0	8.5	0	2	0	14276.5774	0.0072
10.5	0	2	0	9.5	0	2	0	14276.6980	−0.0006
11.5	0	2	0	10.5	0	2	0	14276.8332	0.0008
12.5	0	2	0	11.5	0	2	0	14276.9759	0.0044
13.5	0	2	0	12.5	0	2	0	14277.1088	−0.0072
14.5	0	2	0	13.5	0	2	0	14277.2687	0.0028
16.5	0	2	0	15.5	0	2	0	14277.5786	−0.0036
0.5	0	2	0	0.5	0	1	0	14275.6498	0.0011
1.5	0	2	0	1.5	0	1	0	14275.7262	−0.0023
2.5	0	2	0	2.5	0	1	0	14275.8171	0.0038
3.5	0	2	0	3.5	0	1	0	14275.9082	0.0049
4.5	0	2	0	4.5	0	1	0	14275.9982	−0.0003
5.5	0	2	0	5.5	0	1	0	14276.0986	−0.0002
6.5	0	2	0	6.5	0	1	0	14276.2060	0.0018
7.5	0	2	0	7.5	0	1	0	14276.3143	−0.0006
8.5	0	2	0	8.5	0	1	0	14276.4274	−0.0034
9.5	0	2	0	9.5	0	1	0	14276.5554	0.0034
10.5	0	2	0	10.5	0	1	0	14276.6807	0.0022
11.5	0	2	0	11.5	0	1	0	14276.8112	0.0009
12.5	0	2	0	12.5	0	1	0	14276.9464	−0.0011
13.5	0	2	0	13.5	0	1	0	14277.0867	−0.0033
14.5	0	2	0	14.5	0	1	0	14277.2329	−0.0051
16.5	0	2	0	16.5	0	1	0	14277.5563	0.0058
SrSH				*B*2*A*″–*X*2*A*′					
1.5	0	1	1	1.5	0	1	0	14811.6946	−0.0006
2.5	0	1	1	2.5	0	1	0	14811.7967	−0.0019
3.5	0	1	1	3.5	0	1	0	14811.9061	0.0006
4.5	0	1	1	4.5	0	1	0	14812.0189	0.0030
5.5	0	1	1	5.5	0	1	0	14812.1345	0.0046
6.5	0	1	1	6.5	0	1	0	14812.2493	0.0020
7.5	0	1	1	7.5	0	1	0	14812.3724	0.0042
8.5	0	1	1	8.5	0	1	0	14812.4953	0.0028
9.5	0	1	1	9.5	0	1	0	14812.6290	0.0088
10.5	0	1	1	10.5	0	1	0	14812.7568	0.0056
11.5	0	1	1	11.5	0	1	0	14812.8903	0.0048

(*continued*)

Table S1. Continued.

J	GAM	F	Ka	J	GAM	F	Ka	OBS	OMC
12.5	0	1	1	12.5	0	1	0	14813.0169	−0.0062
1.5	0	1	1	2.5	0	2	0	14810.7426	−0.0029
2.5	0	1	1	3.5	0	2	0	14810.4695	0.0005
3.5	0	1	1	4.5	0	2	0	14810.1946	−0.0015
4.5	0	1	1	5.5	0	2	0	14809.9267	0.0000
5.5	0	1	1	6.5	0	2	0	14809.6598	−0.0010
6.5	0	1	1	7.5	0	2	0	14809.3988	0.0004
7.5	0	1	1	8.5	0	2	0	14809.1418	0.0023
8.5	0	1	1	9.5	0	2	0	14808.8858	0.0018
1.5	0	1	1	0.5	0	2	0	14811.6946	−0.0035
2.5	0	1	1	1.5	0	2	0	14811.7967	−0.0067
3.5	0	1	1	2.5	0	2	0	14811.9061	−0.0061
4.5	0	1	1	3.5	0	2	0	14812.0230	−0.0016
5.5	0	1	1	4.5	0	2	0	14812.1416	0.0011
6.5	0	1	1	5.5	0	2	0	14812.2617	0.0019
7.5	0	1	1	6.5	0	2	0	14812.3859	0.0033
8.5	0	1	1	7.5	0	2	0	14812.5138	0.0050
9.5	0	1	1	8.5	0	2	0	14812.6463	0.0079
10.5	0	1	1	9.5	0	2	0	14812.7770	0.0056
11.5	0	1	1	10.5	0	2	0	14812.9156	0.0080
12.5	0	1	1	11.5	0	2	0	14813.0394	−0.0077
1.5	1	1	1	0.5	0	1	0	14811.8884	0.0014
2.5	1	1	1	1.5	0	1	0	14812.1817	0.0004
3.5	1	1	1	2.5	0	1	0	14812.4781	−0.0011
4.5	1	1	1	3.5	0	1	0	14812.7770	−0.0035
5.5	1	1	1	4.5	0	1	0	14813.0882	0.0029
6.5	1	1	1	5.5	0	1	0	14813.3908	−0.0028
7.5	1	1	1	6.5	0	1	0	14813.7081	0.0028
8.5	1	1	1	7.5	0	1	0	14814.0194	−0.0010
9.5	1	1	1	8.5	0	1	0	14814.3403	0.0015
10.5	1	1	1	9.5	0	1	0	14814.6638	0.0033
1.5	1	1	1	1.5	0	2	0	14811.3119	−0.0053
2.5	1	1	1	2.5	0	2	0	14811.2252	−0.0065
3.5	1	1	1	3.5	0	2	0	14811.1448	−0.0048
4.5	1	1	1	4.5	0	2	0	14811.0648	−0.0063
5.5	1	1	1	5.5	0	2	0	14810.9962	0.0001
6.5	1	1	1	6.5	0	2	0	14810.9234	−0.0011
7.5	1	1	1	7.5	0	2	0	14810.8520	−0.0044
8.5	1	1	1	8.5	0	2	0	14810.7868	−0.0049
9.5	1	1	1	9.5	0	2	0	14810.7277	−0.0027
10.5	1	1	1	10.5	0	2	0	14810.6712	−0.0011
11.5	1	1	1	11.5	0	2	0	14810.6134	−0.0041
12.5	1	1	1	12.5	0	2	0	14810.5667	0.0008
13.5	1	1	1	13.5	0	2	0	14810.5163	−0.0011
14.5	1	1	1	14.5	0	2	0	14810.4695	−0.0024
15.5	1	1	1	15.5	0	2	0	14810.4312	0.0018
1.5	1	1	1	2.5	0	1	0	14811.3119	−0.0005
2.5	1	1	1	3.5	0	1	0	14811.2252	0.0003
3.5	1	1	1	4.5	0	1	0	14811.1448	0.0038
4.5	1	1	1	5.5	0	1	0	14811.0648	0.0043
5.5	1	1	1	6.5	0	1	0	14810.9894	0.0058
6.5	1	1	1	7.5	0	1	0	14810.9099	−0.0002
7.5	1	1	1	8.5	0	1	0	14810.8360	−0.0041
8.5	1	1	1	9.5	0	1	0	14810.7721	−0.0014

Table S1. Continued.

J	GAM	F	Ka	J	GAM	F	Ka	OBS	OMC
9.5	1	1	1	10.5	0	1	0	14810.7093	−0.0009
10.5	1	1	1	11.5	0	1	0	14810.6466	−0.0036
11.5	1	1	1	12.5	0	1	0	14810.5975	0.0040
12.5	1	1	1	13.5	0	1	0	14810.5409	0.0010
13.5	1	1	1	14.5	0	1	0	14810.4894	−0.0001
14.5	1	1	1	15.5	0	1	0	14810.4417	−0.0005
15.5	1	1	1	16.5	0	1	0	14810.3939	−0.0039
1.5	0	2	1	0.5	0	1	0	14827.1661	−0.0033
3.5	0	2	1	2.5	0	1	0	14827.7671	0.0020
4.5	0	2	1	3.5	0	1	0	14828.0717	0.0041
5.5	0	2	1	4.5	0	1	0	14828.3699	−0.0033
6.5	0	2	1	5.5	0	1	0	14828.6823	0.0004
0.5	1	2	1	0.5	0	2	0	14826.6811	0.0016
1.5	0	2	1	1.5	0	2	0	14826.5986	−0.0010
2.5	0	2	1	2.5	0	2	0	14826.5138	−0.0022
3.5	0	2	1	3.5	0	2	0	14826.4359	0.0004
4.5	0	2	1	4.5	0	2	0	14826.3600	0.0018
5.5	0	2	1	5.5	0	2	0	14826.2887	0.0048
6.5	0	2	1	6.5	0	2	0	14826.2161	0.0032
7.5	0	2	1	7.5	0	2	0	14826.1485	0.0035
8.5	0	2	1	8.5	0	2	0	14826.0816	0.0012
9.5	0	2	1	9.5	0	2	0	14826.0199	0.0008
10.5	0	2	1	10.5	0	2	0	14825.9603	−0.0008
11.5	0	2	1	11.5	0	2	0	14825.9037	−0.0028
12.5	0	2	1	12.5	0	2	0	14825.8561	0.0008
13.5	0	2	1	13.5	0	2	0	14825.8052	−0.0025
14.5	0	2	1	14.5	0	2	0	14825.7573	−0.0062
15.5	0	2	1	15.5	0	2	0	14825.7271	0.0041
16.5	0	2	1	16.5	0	2	0	14825.6823	−0.0038
17.5	0	2	1	17.5	0	2	0	14825.6577	0.0048
0.5	1	2	1	1.5	0	1	0	14826.6811	0.0045
1.5	0	2	1	2.5	0	1	0	14826.5986	0.0038
2.5	0	2	1	3.5	0	1	0	14826.5138	0.0045
3.5	0	2	1	4.5	0	1	0	14826.4313	0.0044
4.5	0	2	1	5.5	0	1	0	14826.3502	0.0026
5.5	0	2	1	6.5	0	1	0	14826.2739	0.0024
6.5	0	2	1	7.5	0	1	0	14826.1999	0.0014
7.5	0	2	1	8.5	0	1	0	14826.1313	0.0026
8.5	0	2	1	9.5	0	1	0	14826.0639	0.0017
9.5	0	2	1	10.5	0	1	0	14826.0003	0.0014
10.5	0	2	1	11.5	0	1	0	14825.9418	0.0028
11.5	0	2	1	12.5	0	1	0	14825.8828	0.0003
12.5	0	2	1	13.5	0	1	0	14825.8237	−0.0057
13.5	0	2	1	14.5	0	1	0	14825.7745	−0.0053
14.5	0	2	1	15.5	0	1	0	14825.7271	−0.0066
15.5	0	2	1	16.5	0	1	0	14825.6858	−0.0055
16.5	0	2	1	17.5	0	1	0	14825.6577	0.0052
0.5	0	2	1	1.5	0	2	0	14826.2995	−0.0059
1.5	1	2	1	2.5	0	2	0	14826.0199	0.0054
2.5	1	2	1	3.5	0	2	0	14825.7271	−0.0062
3.5	1	2	1	4.5	0	2	0	14825.4500	−0.0051
0.5	0	2	1	0.5	0	1	0	14826.8668	−0.0084
1.5	1	2	1	1.5	0	1	0	14826.9652	0.0011
2.5	1	2	1	2.5	0	1	0	14827.0636	0.0008

(*continued*)

Table S1. Continued.

J	GAM	F	*Ka*	*J*	GAM	F	*Ka*	OBS	OMC
3.5	1	2	1	3.5	0	1	0	14827.1661	0.0017
4.5	1	2	1	4.5	0	1	0	14827.2727	0.0036
5.5	1	2	1	5.5	0	1	0	14827.3760	−0.0007
6.5	1	2	1	6.5	0	1	0	14827.4807	−0.0065
7.5	1	2	1	7.5	0	1	0	14827.5998	−0.0010
8.5	1	2	1	8.5	0	1	0	14827.7167	−0.0007
9.5	1	2	1	9.5	0	1	0	14827.8372	0.0003
10.5	1	2	1	10.5	0	1	0	14827.9603	0.0008
11.5	1	2	1	11.5	0	1	0	14828.0870	0.0019
12.5	1	2	1	12.5	0	1	0	14828.2149	0.0011
13.5	1	2	1	13.5	0	1	0	14828.3465	0.0009
14.5	1	2	1	14.5	0	1	0	14828.4843	0.0039
15.5	1	2	1	15.5	0	1	0	14828.6171	−0.0014
16.5	1	2	1	16.5	0	1	0	14828.7635	0.0038
17.5	1	2	1	17.5	0	1	0	14828.9000	−0.0041
1.5	1	2	1	0.5	0	2	0	14826.9652	−0.0018
2.5	1	2	1	1.5	0	2	0	14827.0632	−0.0044
3.5	1	2	1	2.5	0	2	0	14827.1682	−0.0030
4.5	1	2	1	3.5	0	2	0	14827.2758	−0.0019
5.5	1	2	1	4.5	0	2	0	14827.3846	−0.0026
6.5	1	2	1	5.5	0	2	0	14827.5003	0.0006
7.5	1	2	1	6.5	0	2	0	14827.6134	−0.0018
8.5	1	2	1	7.5	0	2	0	14827.7339	0.0002
9.5	1	2	1	8.5	0	2	0	14827.8556	0.0004
10.5	1	2	1	9.5	0	2	0	14827.9799	0.0002
11.5	1	2	1	10.5	0	2	0	14828.1091	0.0019
12.5	1	2	1	11.5	0	2	0	14828.2371	−0.0007
13.5	1	2	1	12.5	0	2	0	14828.3699	−0.0016
14.5	1	2	1	13.5	0	2	0	14828.5101	0.0018
15.5	1	2	1	14.5	0	2	0	14828.6466	−0.0017
16.5	1	2	1	15.5	0	2	0	14828.7911	−0.0003
17.5	1	2	1	16.5	0	2	0	14828.9369	−0.0008
1.5	0	2	0	0.5	0	2	0	14809.7608	−0.0048
2.5	0	2	0	1.5	0	2	0	14809.8800	−0.0049
3.5	0	2	0	2.5	0	2	0	14810.0064	0.0001
4.5	0	2	0	3.5	0	2	0	14810.1303	0.0005
5.5	0	2	0	4.5	0	2	0	14810.2538	−0.0016
6.5	0	2	0	5.5	0	2	0	14810.3846	0.0015
7.5	0	2	0	6.5	0	2	0	14810.5163	0.0034
8.5	0	2	0	7.5	0	2	0	14810.6466	0.0018
9.5	0	2	0	8.5	0	2	0	14810.7721	−0.0068
10.5	0	2	0	9.5	0	2	0	14810.9099	−0.0051
0.5	0	2	0	1.5	0	2	0	14809.0815	0.0039
1.5	0	2	0	2.5	0	2	0	14808.8121	−0.0009
2.5	0	2	0	3.5	0	2	0	14808.5501	−0.0004
3.5	0	2	0	4.5	0	2	0	14808.2919	0.0017
4.5	0	2	0	5.5	0	2	0	14808.0323	0.0004
5.5	0	2	0	6.5	0	2	0	14807.7789	0.0031
6.5	0	2	0	7.5	0	2	0	14807.5245	0.0027
7.5	0	2	0	8.5	0	2	0	14807.2660	−0.0039
8.5	0	2	0	9.5	0	2	0	14807.0225	0.0024
9.5	0	2	0	10.5	0	2	0	14806.7737	0.0013
0.5	0	2	0	0.5	0	1	0	14809.6448	−0.0026
1.5	0	2	0	1.5	0	1	0	14809.7608	−0.0019

Table S1. Continued.

J	GAM	F	*Ka*	*J*	GAM	F	*Ka*	OBS	OMC
2.5	0	2	0	2.5	0	1	0	14809.8800	−0.0001
3.5	0	2	0	3.5	0	1	0	14810.0005	0.0010
4.5	0	2	0	4.5	0	1	0	14810.1234	0.0023
5.5	0	2	0	5.5	0	1	0	14810.2468	0.0020
6.5	0	2	0	6.5	0	1	0	14810.3711	0.0005
7.5	0	2	0	7.5	0	1	0	14810.4987	0.0002
8.5	0	2	0	8.5	0	1	0	14810.6307	0.0022
10.5	0	2	0	10.5	0	1	0	14810.8987	0.0039
1.5	0	1	0	0.5	0	1	0	14809.8800	−0.0043
2.5	0	1	0	1.5	0	1	0	14810.1558	−0.0017
3.5	0	1	0	2.5	0	1	0	14810.4312	−0.0017
4.5	0	1	0	3.5	0	1	0	14810.7093	−0.0012
5.5	0	1	0	4.5	0	1	0	14810.9894	−0.0010
6.5	0	1	0	5.5	0	1	0	14811.2739	0.0014
7.5	0	1	0	6.5	0	1	0	14811.5556	−0.0013
8.5	0	1	0	7.5	0	1	0	14811.8409	−0.0026
9.5	0	1	0	8.5	0	1	0	14812.1345	0.0019
10.5	0	1	0	9.5	0	1	0	14812.4253	0.0014
11.5	0	1	0	10.5	0	1	0	14812.7229	0.0053
0.5	0	1	0	1.5	0	1	0	14809.4235	0.0031
1.5	0	1	0	2.5	0	1	0	14809.3128	0.0032
2.5	0	1	0	3.5	0	1	0	14809.2033	0.0022
3.5	0	1	0	4.5	0	1	0	14809.1012	0.0065
4.5	0	1	0	5.5	0	1	0	14808.9893	−0.0012
5.5	0	1	0	6.5	0	1	0	14808.8858	−0.0028
0.5	0	1	0	0.5	0	2	0	14809.4235	0.0002
1.5	0	1	0	1.5	0	2	0	14809.3128	−0.0016
2.5	0	1	0	2.5	0	2	0	14809.2033	−0.0045
3.5	0	1	0	3.5	0	2	0	14809.1012	−0.0021
4.5	0	1	0	4.5	0	2	0	14809.0016	0.0005
5.5	0	1	0	5.5	0	2	0	14808.8994	−0.0017
SrSH				*C*2*A*′–*X*2*A*′					
1.5	0	1	0	0.5	0	1	0	15003.3724	−0.0035
2.5	0	1	0	1.5	0	1	0	15003.6018	−0.0056
3.5	0	1	0	2.5	0	1	0	15003.8424	0.0003
4.5	0	1	0	3.5	0	1	0	15004.0796	−0.0006
5.5	0	1	0	4.5	0	1	0	15004.3175	−0.0041
6.5	0	1	0	5.5	0	1	0	15004.5666	0.0003
7.5	0	1	0	6.5	0	1	0	15004.8155	0.0012
8.5	0	1	0	7.5	0	1	0	15005.0646	−0.0010
9.5	0	1	0	8.5	0	1	0	15005.3219	0.0016
10.5	0	1	0	9.5	0	1	0	15005.5793	0.0010
11.5	0	1	0	10.5	0	1	0	15005.8424	0.0028
12.5	0	1	0	11.5	0	1	0	15006.1106	0.0062
13.5	0	1	0	12.5	0	1	0	15006.3820	0.0095
0.5	0	1	0	1.5	0	1	0	15002.9555	0.0005
1.5	0	1	0	2.5	0	1	0	15002.8045	0.0032
2.5	0	1	0	3.5	0	1	0	15002.6532	0.0022
3.5	0	1	0	4.5	0	1	0	15002.5077	0.0037
4.5	0	1	0	5.5	0	1	0	15002.3595	−0.0008
5.5	0	1	0	6.5	0	1	0	15002.2169	−0.0030
6.5	0	1	0	7.5	0	1	0	15002.0796	−0.0032
7.5	0	1	0	8.5	0	1	0	15001.9431	−0.0060
8.5	0	1	0	9.5	0	1	0	15001.8171	−0.0016

(*continued*)

Table S1. Continued.

J	GAM	F	Ka	J	GAM	F	Ka	OBS	OMC
9.5	0	1	0	10.5	0	1	0	15001.6895	−0.0021
10.5	0	1	0	11.5	0	1	0	15001.5682	0.0002
1.5	0	2	0	0.5	0	2	0	15003.4357	0.0000
2.5	0	2	0	1.5	0	2	0	15003.6018	−0.0007
3.5	0	2	0	2.5	0	2	0	15003.7737	0.0010
4.5	0	2	0	3.5	0	2	0	15003.9459	−0.0003
5.5	0	2	0	4.5	0	2	0	15004.1188	−0.0041
6.5	0	2	0	5.5	0	2	0	15004.2980	−0.0050
7.5	0	2	0	6.5	0	2	0	15004.4883	0.0019
8.5	0	2	0	7.5	0	2	0	15004.6729	−0.0003
9.5	0	2	0	8.5	0	2	0	15004.8575	−0.0058
10.5	0	2	0	9.5	0	2	0	15005.0646	0.0079
0.5	0	2	0	1.5	0	2	0	15002.7036	0.0022
1.5	0	2	0	2.5	0	2	0	15002.4870	0.0039
2.5	0	2	0	3.5	0	2	0	15002.2699	0.0017
3.5	0	2	0	4.5	0	2	0	15002.0602	0.0036
4.5	0	2	0	5.5	0	2	0	15001.8507	0.0024
5.5	0	2	0	6.5	0	2	0	15001.6466	0.0033
6.5	0	2	0	7.5	0	2	0	15001.4451	0.0035
7.5	0	2	0	8.5	0	2	0	15001.2464	0.0030
8.5	0	2	0	9.5	0	2	0	15001.0477	−0.0007
9.5	0	2	0	10.5	0	2	0	15000.8519	−0.0049
10.5	0	2	0	11.5	0	2	0	15000.6616	−0.0070
11.5	0	2	0	12.5	0	2	0	15000.4770	−0.0068
0.5	0	1	0	0.5	0	2	0	15002.9555	−0.0024
1.5	0	1	0	1.5	0	2	0	15002.8045	−0.0016
2.5	0	1	0	2.5	0	2	0	15002.6532	−0.0045
3.5	0	1	0	3.5	0	2	0	15002.5077	-0.0049
4.5	0	1	0	4.5	0	2	0	15002.3680	−0.0028
5.5	0	1	0	5.5	0	2	0	15002.2320	−0.0004
6.5	0	1	0	6.5	0	2	0	15002.0937	−0.0035
7.5	0	1	0	7.5	0	2	0	15001.9610	−0.0044
8.5	0	1	0	8.5	0	2	0	15001.8341	−0.0028
9.5	0	1	0	9.5	0	2	0	15001.7110	−0.0008
10.5	0	1	0	10.5	0	2	0	15001.5895	−0.0006
0.5	0	2	0	0.5	0	1	0	15003.2712	0.0000
1.5	0	2	0	1.5	0	1	0	15003.4357	0.0029
2.5	0	2	0	2.5	0	1	0	15003.6018	0.0041
3.5	0	2	0	3.5	0	1	0	15003.7737	0.0077
4.5	0	2	0	4.5	0	1	0	15003.9459	0.0084
5.5	0	2	0	5.5	0	1	0	15004.1188	0.0064
6.5	0	2	0	6.5	0	1	0	15004.2980	0.0075
7.5	0	2	0	7.5	0	1	0	15004.4730	0.0010
8.5	0	2	0	8.5	0	1	0	15004.6514	−0.0055
9.5	0	2	0	9.5	0	1	0	15004.8411	−0.0039
CaSH				*C*2*A*′–*X*2*A*′					
1.5	0	1	0	0.5	0	1	0	16075.3918	−0.0011
2.5	0	1	0	1.5	0	1	0	16075.6661	0.0017
3.5	0	1	0	2.5	0	1	0	16075.9487	0.0048
4.5	0	1	0	3.5	0	1	0	16076.2363	0.0047
5.5	0	1	0	4.5	0	1	0	16076.5274	0.0001
6.5	0	1	0	5.5	0	1	0	16076.8296	−0.0016
7.5	0	1	0	6.5	0	1	0	16077.1429	−0.0003
8.5	0	1	0	7.5	0	1	0	16077.4620	−0.0013

Table S1. Continued.

J	GAM	F	Ka	J	GAM	F	Ka	OBS	OMC
9.5	0	1	0	8.5	0	1	0	16077.7920	0.0005
10.5	0	1	0	9.5	0	1	0	16078.1329	0.0049
0.5	0	1	0	1.5	0	1	0	16074.8462	−0.0005
1.5	0	1	0	2.5	0	1	0	16074.5469	−0.0002
2.5	0	1	0	3.5	0	1	0	16074.2560	0.0004
3.5	0	1	0	4.5	0	1	0	16073.9766	0.0044
4.5	0	1	0	5.5	0	1	0	16073.6951	−0.0018
5.5	0	1	0	6.5	0	1	0	16073.4279	−0.0019
6.5	0	1	0	7.5	0	1	0	16073.1695	−0.0013
7.5	0	1	0	8.5	0	1	0	16072.9220	0.0021
8.5	0	1	0	9.5	0	1	0	16072.6757	−0.0016
1.5	0	2	0	0.5	0	2	0	16075.7920	−0.0019
2.5	0	2	0	1.5	0	2	0	16076.1273	0.0015
3.5	0	2	0	2.5	0	2	0	16076.4629	−0.0029
4.5	0	2	0	3.5	0	2	0	16076.8143	0.0004
5.5	0	2	0	4.5	0	2	0	16077.1737	0.0035
6.5	0	2	0	5.5	0	2	0	16077.5375	0.0030
7.5	0	2	0	6.5	0	2	0	16077.9055	−0.0015
8.5	0	2	0	7.5	0	2	0	16078.2837	−0.0040
0.5	0	2	0	1.5	0	2	0	16074.6253	−0.0017
1.5	0	2	0	2.5	0	2	0	16074.3874	−0.0005
2.5	0	2	0	3.5	0	2	0	16074.1608	0.0039
3.5	0	2	0	4.5	0	2	0	16073.9346	0.0006
4.5	0	2	0	5.5	0	2	0	16073.7197	0.0005
5.5	0	2	0	6.5	0	2	0	16073.5122	−0.0004
6.5	0	2	0	7.5	0	2	0	16073.3135	−0.0006
7.5	0	2	0	8.5	0	2	0	16073.1204	−0.0034
0.5	0	1	0	0.5	0	2	0	16074.8462	−0.0026
1.5	0	1	0	1.5	0	2	0	16074.5469	−0.0037
2.5	0	1	0	2.5	0	2	0	16074.2560	−0.0045
3.5	0	1	0	3.5	0	2	0	16073.9766	−0.0019
4.5	0	1	0	4.5	0	2	0	16073.6989	−0.0057
5.5	0	1	0	5.5	0	2	0	16073.4375	−0.0014
6.5	0	1	0	6.5	0	2	0	16073.1779	−0.0033
7.5	0	1	0	7.5	0	2	0	16072.9345	0.0027
0.5	0	2	0	0.5	0	1	0	16075.4702	0.0008
1.5	0	2	0	1.5	0	1	0	16075.7920	0.0002
2.5	0	2	0	2.5	0	1	0	16076.1273	0.0050
3.5	0	2	0	3.5	0	1	0	16076.4629	0.0020
4.5	0	2	0	4.5	0	1	0	16076.8143	0.0066
5.5	0	2	0	5.5	0	1	0	16077.1626	0.0001
6.5	0	2	0	6.5	0	1	0	16077.5216	−0.0038
7.5	0	2	0	7.5	0	1	0	16077.8982	0.0017
8.5	0	2	0	8.5	0	1	0	16078.2749	−0.0009